6-7-2022

A quantitative model of volume compensation as a mechanism for oscillatory flow of cerebrospinal fluid

Charles F. Babbs

Technical Note

A quantitative model of volume compensation as a mechanism for oscillatory flow of cerebrospinal fluid

Charles F. Babbs, MD, PhD
Weldon School of Biomedical Engineering
Purdue University, West Lafayette Indiana, USA

Abstract

Specifying the exact mechanism driving cyclic, oscillatory flows of cerebrospinal fluid (CSF) through the cerebral ventricles and subarachnoid spaces remains an open problem. Here is a new quantitative hypothesis describing how cyclic expansion and contraction of the cerebral blood volume moves CSF within the closed box of the cranium. As whole brain tissue expands with added blood, volume compensation is provided by partial collapse of the superior sagittal and transverse venous sinuses. The magnitude of the expansion and contraction of whole brain tissue volume can be estimated from the changes in intravascular volume, which in turn can be divided into arterial, venous, and capillary fractions. Each of these volume fractions changes cyclically on a separate time scale. Arterial volume changes at the frequency of the heartbeat. Venous volume changes at the frequency of breathing in response to changes in intrathoracic pressure. Capillary volume changes according to temporal patterns of autoregulation, driven by chemical signals resulting from neural activity, especially during sleep. These volume changes can be predicted from principles of classical anatomy and physiology. In turn, using approximate geometric models of CSF filled spaces, local volumetric flows and flow velocities can be calculated. The calculations imply the existence of cyclic changes in CSF flow at three different frequencies and having three different magnitudes, which are in agreement with observational data in normal humans. Such models can be individualized using routine clinical data and imaging. Further, the predicted tidal movements of CSF over the cerebral convexities would continually refresh fluid drawn into and out of the Virchow-Robbins spaces, providing enhanced clearance of waste products during sleep and during strenuous exercise.

Keywords: 4D MRI, Alzheimer's, amyloid, brain, cerebral aqueduct, cerebral blood volume, choroid plexus, CSF, exercise, fMRI, fourth ventricle, glymphatic, hydrocephalus, Monro-Kellie, oscillations, pulsations, sleep, superior sagittal sinus, subarachnoid space, Virchow-Robbins,

Introduction

Oscillatory expansion and contraction of cerebral blood volume is increasingly being understood as a major driver of the movement of cerebrospinal fluid (CSF) through the cerebral ventricles and subarachnoid spaces[1-3]. Although the adult cranium is a rigid closed box of constant volume; intravascular, and in turn total brain volume, are not constant, but variable on time scales associated with the heartbeat, with respiration, and with periodic changes in whole brain activity. As brain volume increases, brain surfaces expand radially, causing displacement of the CSF. This proposed mechanism of fluid movement may refresh fluid over the cerebral convexities at the entrances of Virchow-Robbins spaces, and thus aid in clearance of toxins by the cerebral equivalent of lymphatic circulation in extracranial body tissues[4,5].

The present paper builds upon the original Monro-Kellie hypothesis[6] and subsequent refinements by Linninger[7], Linge[8], Rey[9], Thomas[10], Yang [3], and their respective coworkers. The goal is to create a quantitative, but still conceptually simple explanation of tidal movements of CSF, caused by changes in cerebral blood volume and synchronized either with the cardiac cycle, the respiratory cycle, or cycles of autoregulatory vasodilation in the brain. The key insight is that intravascular, cerebral blood volume can change in three different ways on three different time scales. Smallest are changes in intraarterial blood volume that happen at cardiac frequencies. They are caused by pulsations in arterial blood pressure. Next largest are changes in intravenous blood volume that happen at respiratory frequencies. They are caused by oscillations in central venous blood pressure in the chest during breathing. Largest are changes in intracapillary blood volume that happen at slower frequencies. These autoregulatory changes are coupled to cyclic changes in electrical activity and metabolism of the brain, especially during sleep. The magnitudes of CSF flow during the respective half-cycles are related roughly to the total volume expansion (or contraction) divided by the half cycle time or half period during which blood volume is changing.

The next key insight is that as total cerebral blood volume expands and contracts, the large venous sinuses compensate for the changing whole brain volume, so that at the brain expands, the venous sinuses, having low internal pressure, partially collapse, expelling blood into the jugular veins and chest, so that total intracranial volume remains constant. Expansion of internal surfaces of the cerebral ventricles pushes CSF out through the foramina of Luschka and Magendie into the outer subarachnoid space. Expansion of the external surfaces of the cerebellum and cerebral cortex further compresses CSF to create circumferential flow. The incompressible CSF moves tidally through complex channels and over cortical surfaces, ultimately displacing low pressure blood within the venous sinuses. These oscillatory flows are separate from, and generally larger than the hour-by-hour production and absorption of CSF by the choroid plexus and arachnoid granulations[11].

The forgoing mechanism of Monro-Kellie pulsation can be dissected and analyzed in terms of classical physiology. Then from the known classical anatomy of CSF containing compartments, it should be possible to create quantitative estimations of oscillatory CSF flow through the compartments for a standard normal human. Further, from individual patient physiology and anatomy, it should be possible to create similar individualized models and predictions of oscillatory flows in multiple CSF filled spaces.

Methods

The present analysis includes the following steps. The first step is to estimate cyclic changes in brain blood volume, and in turn, total brain volume at cardiac, respiratory, and sleep-associated autoregulatory frequencies. The second step is to characterize the relation between cyclic changes in brain volume and corresponding movement of internal and external brain surfaces through available anatomic pathways for CSF flow. The last step is to compute CSF flow velocities in particular fluid filled channels in and around the brain in terms of local volumetric flow divided by local cross-sectional area perpendicular to the flow. In discussion of the first step,variables are described in terms of rounded textbook normal values and whole number fractions for clarity and concreteness.

Fluid compartments in the brain

We begin with the concept of body fluid compartments from medicine and physiology[12]. One can partition total brain volume into dry volume (~ 1/3) and wet volume (~ 2/3). The wet volume is the cerebral analog of total body water. This fluid compartment can be further partitioned into intracellular, interstitial, and intravascular fractions, as shown in Figure 1. The intracellular fraction is roughly 2/3 of the total fluid volume. The extracellular fraction is roughly 1/3 of total fluid volume. The interstitial fraction is roughly (2/3)*(1/3) = 2/9 of total fluid volume. The intravascular fraction is roughly (1/3)*(1/3) = 1/9 of total fluid volume.

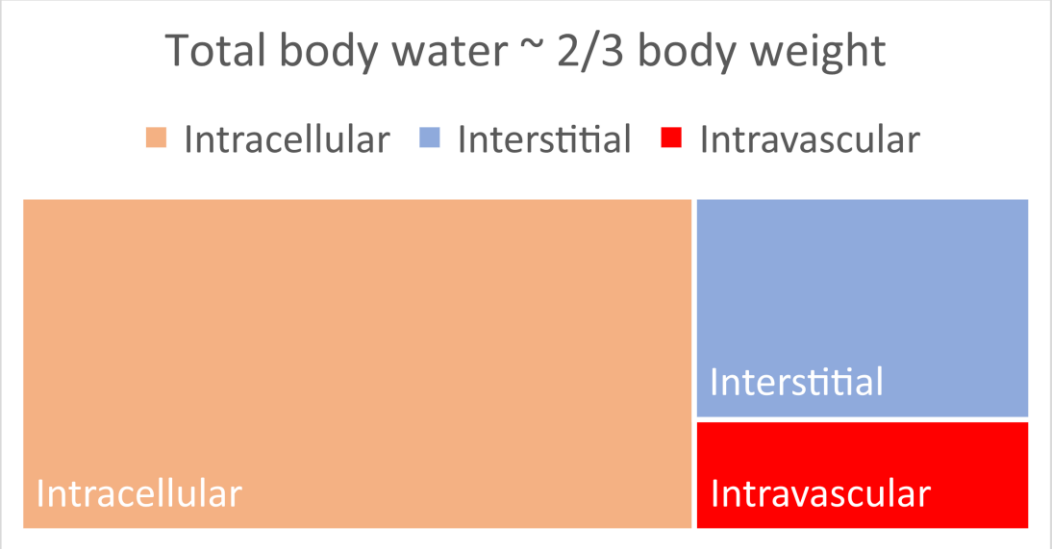

Figure 1. *Classical subdivisions of body water into intracellular, interstitial, and intravascular compartments.*

In turn, the intravascular compartment can be subdivided into volume fractions corresponding approximately to arteries (1/6)*(1/9) = 1/54 of total fluid volume, to veins (2/6)*(1/9) = 1/27 of total fluid volume, and to capillaries (3/6)*(1/9) = 1/18 of total fluid volume.

Cyclic changes in blood volume and in total brain volume coupled to the heartbeat, respiration, and cycles of hyperemia during sleep

Each fraction of cerebral blood volume is subject to normal cyclic variations in response to distinct physiological and biomechanical mechanisms. The arterial sub-fraction expands and contracts at cardiac frequency with the arterial pulse. In a horizontal subject the venous sub-fraction expands and contracts at the respiratory frequency according to changes in intrathoracic pressure. The capillary sub-fraction expands and contracts at a frequency slower than respiration with changes in arteriolar muscle tone and caliber in response to local metabolic activity and oxygen demand, most evident during sleep[13]. The changes in capillary flow occur in response to chemical autoregulatory factors such as carbon dioxide, ADP, and pH[12]. Using this segmentation of cerebral blood volume, one can go on to estimate the magnitudes of the corresponding volume changes on the basis of textbook physiology[12].

Cardiac changes: As revealed by ultrasonic scanning and other methods, the diameters of large arteries change about 5 percent with each pulse. Noting that pulsations decrease in medium and smaller arteries as pressure falls and viscous drag increases, one can estimate that average sized arterial pulsations are roughly 2%. (Empirical data by Thomas[10] suggest 1.7%.) In turn, the internal volumes of the arteries change by about 4 percent or 1/25. For arterial volume fractions of 1/54, as above, the pulsatile change would be (1/25)*(1/54) = 1/1350. At a heart rate of 60/min, each such expansion or contraction phase would last about 0.5 seconds.

Respiratory changes: Diameters of larger veins vary in response to changes in central venous pressure, corresponding to roughly ± 3 mmHg during normal quiet breathing[12]. For mean intracranial venous pressures of about 10 mmHg, as one would expect in a supine subject in an MRI scanner for example, the intravenous volume would change by about 30 percent or 1/3. For venous volume fractions of 1/27, as above, the pulsatile change would be (1/3)*(1/27) = 1/81. At a respiratory rate of 15/min, each such expansion or contraction phase would last about 2 seconds.

Autoregulatory changes: The differences between tissue blood volume in the resting state and tissue blood volume during activity are relatively large. The increased blood volume is contained mostly within capillaries[14]. For example, if tissue blood capillary volume doubles, both because of increased flow in open capillaries and filling of parallel capillaries channels, and if local capillary volume is one half of local blood volume, then the total volume would increase by 150 percent from 1/9 to 3/18 or $1/6^{th}$ of tissue fluid volume. As shown by Yang and coworkers[3], during sleep cyclic changes in brain activity (EEG) and corresponding blood oxygen level (BOLD) determinations vary during the onset and offset ramps of autoregulatory vasodilation and vasoconstriction. The durations of each capillary expansion or contraction phase appear to last about 10 seconds, in keeping with observed lags in BOLD fMRI responses

to intense mental activity[15]. Note that total cerebral blood volume changes only during expansion and contraction of capillary volume, not during steady expansion and steady increased blood flow[3]. Only periods in which total blood volume is changing contain a flow signal.

In summary, cyclic changes in the fraction of brain tissue water are expected to occur with separate and distinctive amplitudes and frequencies shown in Table 1. The fractional change rate in column 4 is the fractional change in total water volume divided by the half-cycle duration (expansion or contraction time). The relative change rate in column 5 is the fractional change rate divided by the largest fractional change rate. There are small, medium, and large amplitude pulsations occurring at high, medium, and low frequencies, respectively.

The forgoing fractional changes in tissue fluid volume can be easily converted to fractional changes in total tissue volume, assuming that fluid volume accounts for 2/3 of total tissue volume. The resulting values are shown in Table 2. It will be these values, representing cyclic expansion or contraction of whole brain tissue that drive the subsequent calculations of CSF movement.

Table 1. Predicted approximate magnitudes of dynamic changes in brain fluid volume

	Fractional change in brain water	Absolute magnitude	Change duration (sec)	Fractional change rate (1/sec)	Relative change rate
Arteries	± 1/1350	0.00074	0.5	± 0.00148	± 0.09
Veins	± 1/81	0.01235	2	± 0.00618	± 0.37
Capillaries	± 3/18	0.16666	10	± 0.01667	± 1.00

Table 2. Predicted approximate magnitudes of dynamic changes in total tissue volume, assuming total body water = 2/3 total tissue volume

	Fractional change in volume, ϕ	Absolute magnitude, of ϕ	Change duration (sec)	Fractional change rate (1/sec)	Relative change rate
Arteries	± (2/3)/1350	0.00049	0.5	± 0.00099	± 0.09
Veins	± (2/3)/81	0.00823	2	± 0.00412	± 0.37
Capillaries	± 2/18	0.11111	10	± 0.01111	± 1.00

From changes in volume to changes in linear dimensions

To model movement of CSF in response to changes in brain volume, one needs to relate the change in whole tissue volume to changes in linear dimensions of the brain. These changes produce displacement of the surface areas of the cortex externally, and of the lateral ventricles internally. From the perspective of fluid flow, the resulting volume displacements of CSF can be viewed as defined flow or current sources, rather than defined pressure sources. The corresponding downstream fluid flow is analogous to the flow of electricity in a circuit having a defined current source. In such a circuit, the total downstream flow is—within limits—independent of the downstream resistance. Figure 2 illustrates a simple geometric scheme for relating surface expansion to volume expansion in the brain.

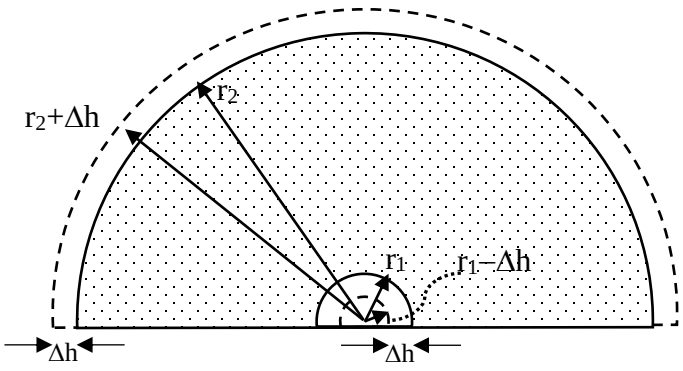

Figure 2. *Simple geometric models of the brain structures having concentric average radii r_1 and r_2 . Hemispheres are used to represent the cerebrum. A whole sphere is used to represent the cerebellum with $r_2 = 0$. Concentric cylinders of constant length, L, are used to represent the midbrain, where r_2 represents the average radius of the midbrain, and where r_1 represents the radius of the cerebral aqueduct. Dashed curves show expansion (exaggerated) caused by increased blood volume. In these models the inner radius, r_1 , shrinks and outer radius, r_2 , expands by a corresponding increment, Δh , for each brain region.*

Cerebral cortex: In this simple model the cerebral cortex is considered roughly hemispherical in shape with average outer radius, r_2 . Each lateral ventricle is considered as a CSF filled quarter sphere with average radius r_1 , and the two lateral ventricular spaces constitute a hemisphere. The volume between the radii r_1 and r_2 represents whole cerebral tissue volume. The surfaces of the inner and outer hemispheres represent the outer cortical surface and the inner lateral ventricular surfaces, respectively. In this model one can size r_1 to correspond either to the combined volumes or the combined surface areas of the first and second ventricles.

The question is, what is the relation between the inner and outer radial expansions of tissue volumes, Δh in Figure 2, and the fractional increases in regional brain volumes. Here, we assume for simplicity equal expansion, Δh , in both inner and outer directions. The volume of outer shell expansion, which pushes CSF into the subarachnoid space is

$$\Delta V_o = 2\pi r_2^2 \Delta h \,, \tag{1a}$$

and the volume of inner shell expansion, which squeezes CSF in the cerebral ventricles is

$$\Delta V_i = 2\pi r_1^2 \Delta h \,. \tag{2a}$$

The fractional expansion in <u>total</u> tissue volume for the hemisphere is

$$\phi = \frac{\Delta V_o + \Delta V_i}{\frac{2\pi}{3}(r_2^3 - r_1^3)} = \frac{2\pi(r_2^2 + r_1^2)\Delta h}{\frac{2\pi}{3}(r_2^3 - r_1^3)} = \frac{3(r_2^2 + r_1^2)\Delta h}{r_2^3 - r_1^3} \,. \tag{3a}$$

Solving for Δh, the surface expansion distance is

$$\Delta h = \frac{\phi}{3} \cdot \frac{r_2^3 - r_1^3}{r_2^2 + r_1^2} \,, \tag{4a}$$

and for $r_2 > 3r_1$, as is very likely in practice for human brain,

$$\Delta h \approx \frac{\phi}{3} r_2 \,, \tag{5a}$$

which is sufficiently accurate for the purpose of the present mathematical model. In this case the fine points concerning the estimation of r_1 are largely irrelevant.

Cerebellum: The cerebellum is considered roughly spherical in shape with a single average outer radius, r_2. For the cerebellum $r_1 = 0$. In this case the expression $\Delta h \approx \frac{\phi}{3} r_2$ is also valid for the cerebellum, using the average cerebellar radius for r_2.

Medulla and spinal cord: Next consider the sketch in Figure 2 to represent, not concentric hemispherical surfaces, but concentric cylindrical surfaces of length, L. This geometry approximates that of the brainstem, as well as the caudal parts of the midbrain. The cylindrical analogs of Equations (1a) through (5a) are

$$\Delta V_o = 2\pi r_2 L \, \Delta h \,, \tag{1b}$$

and

$$\Delta V_i = 2\pi r_1 L \Delta h \,. \tag{2b}$$

The fractional expansion in total tissue volume is

$$\phi = \frac{\Delta V_o + \Delta V_i}{\pi(r_2^2 - r_1^2)L} = \frac{2\pi(r_2 + r_1)\Delta h}{\pi(r_2^2 - r_1^2)} = \frac{2(r_2 + r_1)\Delta h}{r_2^2 - r_1^2} \,, \tag{3b}$$

so that the surface expansion distance is

$$\Delta h = \frac{\phi}{2} \cdot \frac{r_2^2 - r_1^2}{r_2 + r_1} \ , \qquad (4b)$$

and, as before, for $r_2 > 3r_1$, as is very likely in practice for human brain,

$$\Delta h \approx \frac{\phi}{2} r_2 \ , \qquad (5b)$$

for cylindrical geometry.

Calculation of local CSF flow and flow velocity

The movement of CSF is assumed to begin in the cerebral ventricles, as their internal surfaces are compressed by whole brain expansion. Flow accumulates without loss from the lateral ventricles to the third ventricle, through the cerebral aqueduct, into the 4th ventricle, and exits though the foramina of Luschka and Magendie, as shown in Figure 3(a). Because the thin roof of the 4th ventricle provides strain relief for circumferential compression, and also because of venting through the foramina, the net compression volume change in the 4th ventricle is considered to be zero, so that the 4th ventricle acts as a simple conduit. Thereafter CSF is compressed against the rigid skull of the posterior fossa and cranium by outward expansion of the cerebellum and cerebral hemispheres respectively, as shown in Figure 3(b). This outward expansion creates additional volume flow. Movement of CSF happens because of compensatory indentation of the superior sagittal sinus and venous sinuses. Local flows f_1, f_2, …. f_7 in Figure 3 are produced by the product of local surface areas, S_1, S_2, S_3, S_4, … S_7 , and amounts of radial movement, Δh_1, Δh_2, Δh_3, …. Δh_7 , during each particular period of compression or relaxation.

Since volume is conserved and since the outer boundaries are rigid, the total volumetric flow accumulates in the system. The only volume compensation for expanding brain tissue is provided by indentation of the superior sagittal sinus and the transverse sinuses. Local flow velocities in compartment, n , are determined by the aggregate total flow, f_1,+ f_2, ….+ f_n , divided by the local cross sections, A_n , perpendicular to flow. Hence incremental flow, local aggregate flow, and local flow velocity in compartment, n , are computed as

$$f_n = S_n \frac{\Delta h_n}{\Delta t} \ , \qquad (6)$$

$$\Sigma f_n = \sum_1^n f_n \ , \qquad (7)$$

$$v_n = \frac{\Sigma f_n}{A_n} \ , \qquad (8)$$

where variable A_n represents the cross sectional area of compartment, n , perpendicular to flow, f_n .

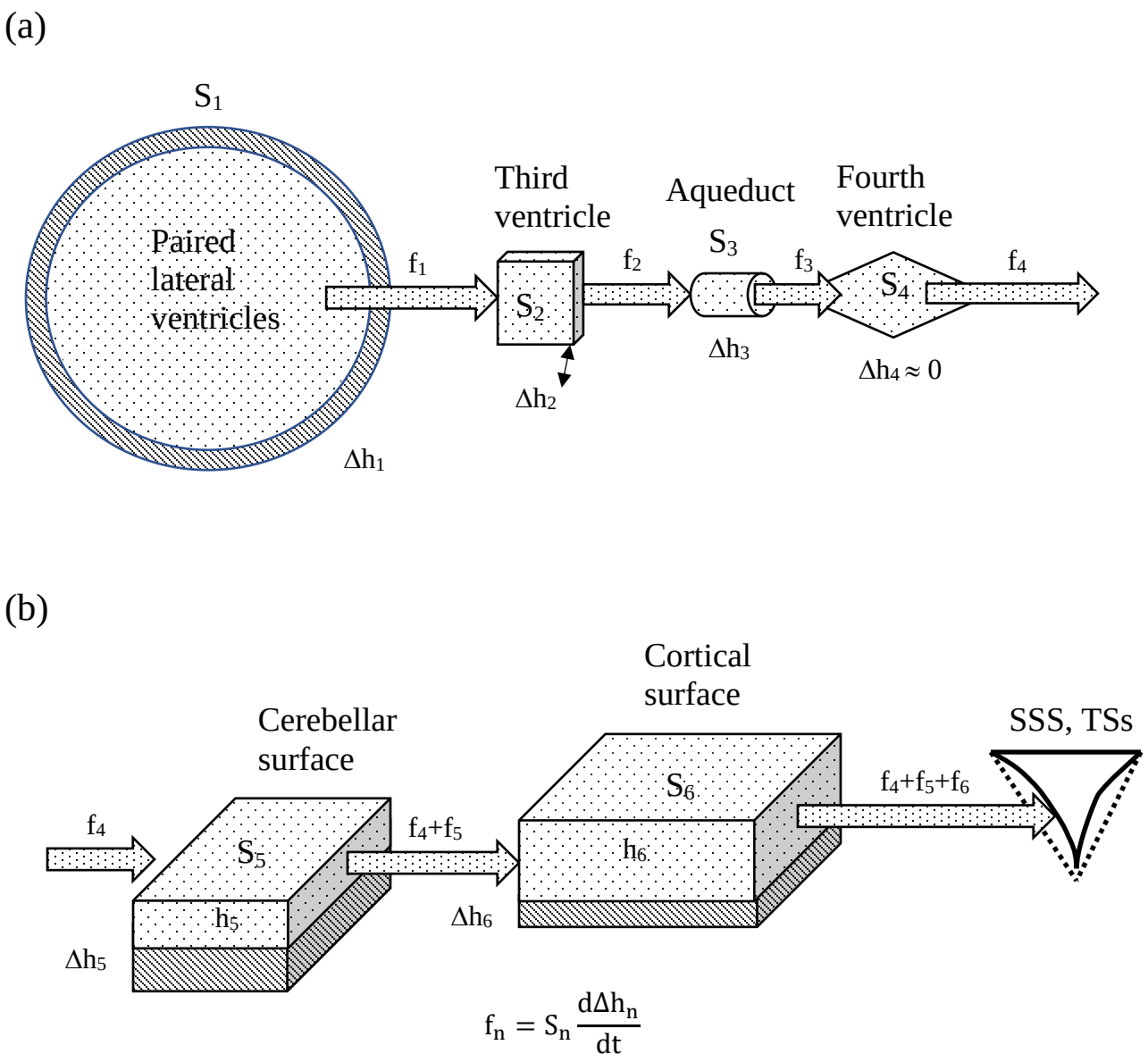

Figure 3. *Conceptual model of flow in the cerebral ventricles (a) and in the subarachnoid space over surfaces of the brain (b). Variables S indicate surface areas that move with brain swelling and squeeze CSF. The thin roof of the 4th ventricle provides strain relief so there is no net squeezing ($\Delta h_4 \approx 0$). Displaced incompressible CSF ultimately pushes the soft walls of the superior sagittal sinus (SSS) and transverse sinuses (TSs) inward to provide volume compensation, forcing blood into the neck and chest, such that the net change in intracranial volume is zero. Flow accumulates along the general direction of flow over brain surfaces.*

Anatomic parameters and numerical methods

Anatomic parameters for normal adult humans were obtained by mapping images in a standard neuroanatomical atlas to quantitative cross-sectional images of Liang[16]. All calculations were done in a simple Microsoft Excel spreadsheet.

Results

Local changes in CSF flow at cardiac frequencies

Table 3 shows numerical values for model parameters and resulting volumetric flows and flow velocities within and around the brain for cardiogenic pulsations in brain blood volume. Values in columns 1 to 3 represent anatomic data for a normal adult human. The surface compression distance, Δh, is calculated using Equations (1) through (5). The surface compression rate is calculated as $\Delta h/\Delta t$ for half cycle time, Δt . Incremental flow, aggregate flow, and local CSF flow velocity are calculated using Equations (6) through (8). Incremental flow is computed as the product of radially moving surface area, S, and $\Delta h/\Delta t$ (compressed area x velocity). The aggregate flow is computed as the sum of inflow plus local incremental flow. The local flow velocity is computed from the relation: flow velocity = aggregate flow/cross section (Equation (8)). Circumferential flow over the cerebral cortex is computed for a mid-cortical location. Small amplitude flows around the spinal cord are not computed.

In Table 3 movement of CSF is assumed to result from pulsations of arteries and arterioles at cardiac frequencies. For a heart rate of 60/min or 1 Hz, the compression and relaxation times are each about one-half cycle or 0.5 sec in duration. As before in Table 2, the fractional pulsation of whole tissue volume is estimated as $\phi = (2/3)/1350$ or 0.00049. For cardiac pulsations the resulting flow velocities over the surfaces of the cerebral cortex are about 0.1 cm/sec, roughly one tenth as fast as in the narrow cerebral aqueduct.

Table 3. Model parameters at cardiac rate:
volume change fraction $\phi = 0.00049$, compression/expansion time $\Delta t = 0.5$ sec

	Local r_2 (cm)	Surface area S (cm^2)	Cross section normal to flow A (cm^2)	Surface compression distance Δh (cm)	Surface compression rate $\Delta h/dt$ (cm/sec)	Incremental CSF flow f (cm^3/sec)	Aggregate CSF flow Σf (cm^3/sec)	Local CSF flow velocity v (cm/sec)
Lateral ventricles	10	24	---	0.00165	0.00329	0.0790	0.0790	---
Third ventricle	10	8	1	0.00165	0.00329	0.0263	0.1053	0.105
Cerebral aqueduct	2	3	0.1	0.00033	0.00066	0.0020	0.1073	1.073
Mid-fourth ventricle*	0	4	1	0.00000	0.00000	0.0000	0.1073	0.107
2 Cerebellar surfaces	4	24	10	0.00066	0.00132	0.0316	0.1389	0.014
2 Mid Cortical surfaces	10	400	20	0.00165	0.00329	1.3169	1.4558	0.073

* Roof of 4^{th} ventricle provides strain relief.

Local changes in CSF flow at respiratory frequencies

Table 4 shows numerical values for model parameters and resulting volumetric flows and flow velocities within and around the brain for pulsations in brain blood volume coupled to ventilation of the lungs in a horizontal person. This movement of CSF is assumed to result from pulsations of veins within the substance of the brain at respiratory frequencies, driven by respiratory changes in pressure within the chest. For a respiratory rate of 15/min or 0.25 Hz, the compression and relaxation times are about one-half cycle or 2 sec in duration. As before in Table 2, the fractional pulsation of whole tissue volume is estimated as (2/3)/81 or 0.00823. CSF flows at respiratory frequency and volume expansion are larger than those at cardiac frequency and volume expansion. Flow velocities over the surfaces of the cerebral cortex for respiratory related oscillations are about 0.3 cm/sec.

Table 4. Model parameters and calculated CSF flows at respiratory rate: volume change fraction $\phi = 0.00823$, compression/expansion time $\Delta t = 2$ sec;

	Local r_2 (cm)	Surface area S (cm^2)	Cross section normal to flow A (cm^2)	Surface compression distance Δh (cm)	Surface compression rate $\Delta h/dt$ (cm/sec)	Incremental CSF flow f (cm^3/sec)	Aggregate CSF flow Σf (cm^3/sec)	Local CSF flow velocity v (cm/sec)
Lateral ventricles	10	24	---	0.02743	0.01372	0.3292	0.3292	---
Third ventricle	10	8	1	0.02743	0.01372	0.1097	0.4390	0.439
Cerebral aqueduct	2	3	0.1	0.00549	0.00274	0.0082	0.4472	4.472
Mid-fourth ventricle*	0	4	1	0.00000	0.00000	0.0000	0.4472	0.447
2 Cerebellar surfaces	4	24	10	0.01097	0.00549	0.1317	0.5789	0.058
2 Mid Cortical surfaces	10	400	20	0.02743	0.01372	5.4870	6.0658	0.303

* Roof of 4^{th} ventricle provides strain relief

Local changes in CSF flow with autoregulation

Table 5 shows numerical values for model parameters and resulting volumetric flows and flow velocities within and around the brain for changes in brain blood volume coupled to presumed autoregulatory changes during sleep. Movement of CSF is assumed to result from chemically mediated expansion or contraction of capillaries and recruitment or de-recruitment of additional parallel capillary channels over periods lasing several tens of seconds. Resulting flow velocities over the surfaces of the cerebral cortex are about 0.8 cm/sec. This tidal movement is sufficient to completely refresh the CSF overlying cortical penetrating arteries and veins and the accompanying Virchow-Robbins spaces.

Table 5. Model parameters and CSF flows at frequencies of local autoregulation during sleep: volume change fraction $\phi = 0.1111$, compression/expansion time $\Delta t = 10$ sec

	Local r_2 (cm)	Surface area S (cm^2)	Cross section normal to flow A (cm^2)	Surface compression distance Δ_h (cm)	Surface compression rate $\Delta_{h/dt}$ (cm/sec)	Incremental CSF flow f (cm^3/sec)	Aggregate CSF flow Σ_f (cm^3/sec)	Local CSF flow velocity v (cm/sec)
Lateral ventricles	10	24	---	0.37037	0.03704	0.8889	0.8889	---
Third ventricle	10	8	1	0.37037	0.03704	0.2963	1.1852	1.185
Cerebral aqueduct	2	3	0.1	0.07407	0.00741	0.0222	1.2074	12.074
Mid-fourth ventricle*	0	4	1	0.00000	0.00000	0.0000	1.2074	1.207
2 Cerebellar surfaces	4	24	10	0.14815	0.01481	0.3556	1.5630	0.156
2 Mid Cortical surfaces	10	400	20	0.37037	0.03704	14.8148	16.3778	0.819

* Roof of 4^{th} ventricle provides strain relief

Figure 4 is a time domain plot of summed normalized flow values at the level of the 4^{th} ventricle caused by changes in arterial, venous, and capillary blood volume. The maximal flow for autoregulatory cycles is represented by 1.00. The time scale spans 60 seconds. The simulated arterial, venous, and capillary flow signals are computed for sinusoidal waveforms as a function of time, t , plus a separate arbitrary delay, τ_{art} , τ_{vein} , or τ_{cap} , for each component signal. The separate time delay values ensure that the three signals are unsynchronized in a physiologically realistic way. Three distinct cyclic variations in summed flow are evident at three distinct frequencies.

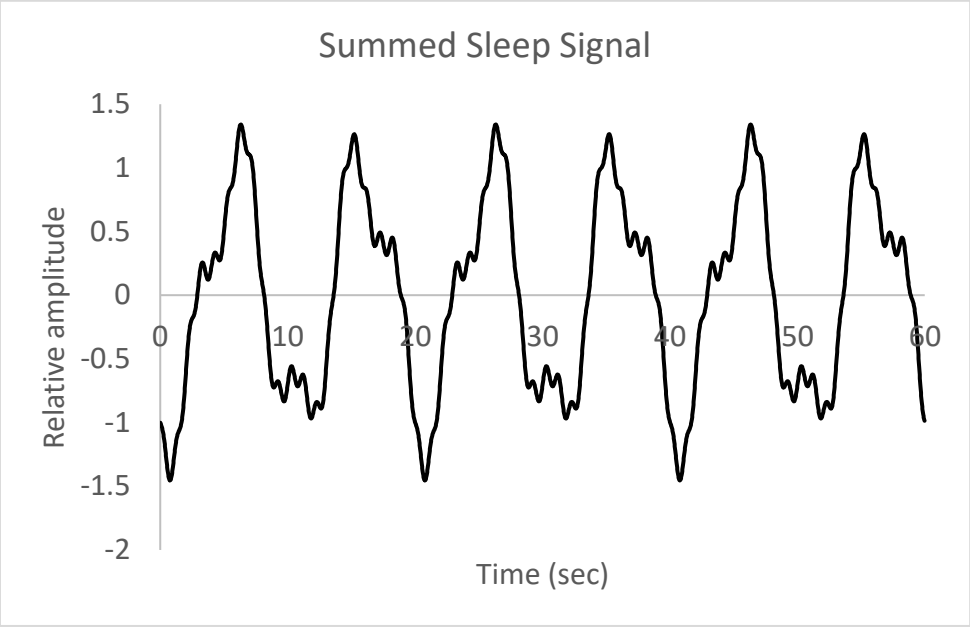

Figure 4. *Relative amplitudes of summed CSF flows (or flow velocities) in the 4th ventricle during sleep. Values on the vertical axis are divided by peak values for the slow wave sleep cycles to allow comparison of amplitudes from arterial, venous, and capillary oscillations. Here bi-directional outflows (> 0) and inflows (< 0) are shown.*

Figure 5 illustrates processing of the raw data in Figure 4 to allow only unidirectional, positive flow, which for technical reasons was measured in the studies of Fultz[13] and of Yang[3] and their respective coworkers. In the awake state the large autoregulatory cycles are absent. There may be relatively constant microvascular vasodilation during the awake state, without the cyclic changes in cerebral blood volume that occur during sleep. With constant capillary blood volume in the awake state there is no signal because it is volume change over time (expansion or contraction of the brain) that drives flow.

The general features of the model flows in Figure 5 are similar to those from experimental studies of fMRI[13] showing three different magnitudes of oscillatory flow at three different frequencies. The numerical values of cardiogenic cerebral aqueduct flow velocity calculated from the present model in Table 3 (~ 1.1 cm/sec) are comparable to those measured by 4DMRI studies in humans by Bradley and coworkers[17] (average unidirectional flow velocity in the cerebral aqueduct ~ 1.5 cm/sec).

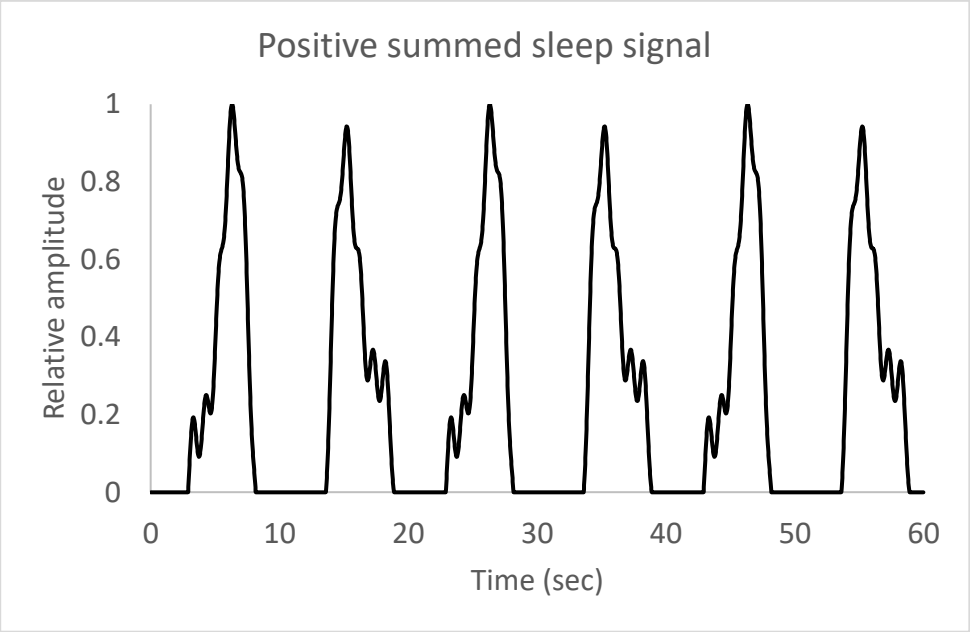

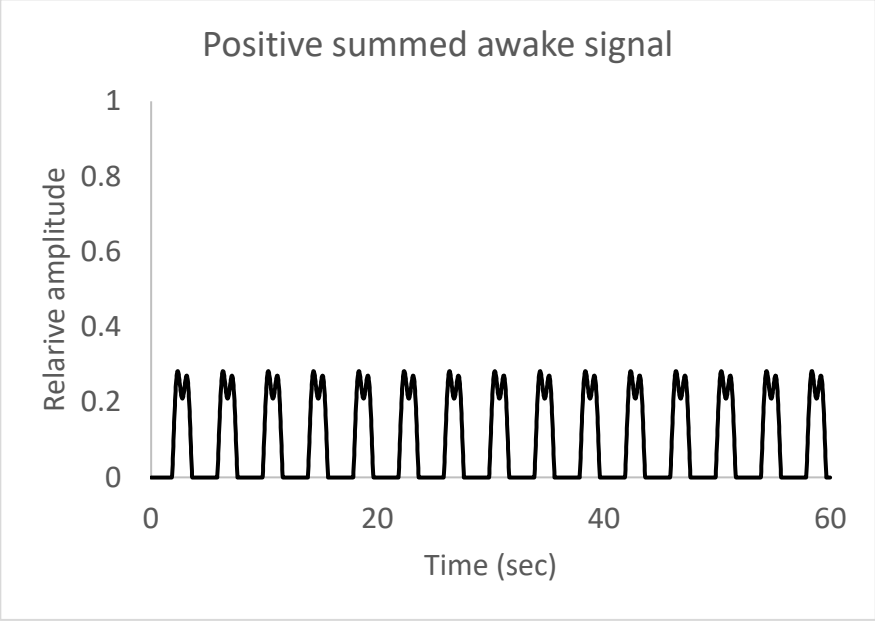

Figure 5. *Unidirectional (positive) amplitudes of summed relative CSF flows (or flow velocities) in the 4th ventricle during sleep in Figure 4. Values are normalized by the maximum time domain signal during sleep. These data simulate those obtained during fMRI studies[13].*

Discussion

The proposed detailed and quantitative mechanism driving oscillatory CSF flow in response to changes in total cerebral blood volume gives a satisfying explanation for some heretofore unexplained complexity of experimental observations. The key to understanding the complexity is segmentation of the total cerebral blood volume into arterial, venous, and capillary sub-compartments. Each sub-compartment has a different volume, and the volumes of each change in different and independent ways. All of the changes, however, can be predicted in terms of classical anatomy and physiology, once it is realized that arteries, veins, and capillaries expand and contract independently via different mechanisms. What is more, the parameters required by the present model can be estimated from standard anatomic atlases and from normal vital signs for a composite normal adult human. In principle, the same parameters can also be estimated from clinical and high-tech imaging data for individual patients.

Although the underlying anatomy for the present model and analysis has been highly simplified, mathematical models such as the one described here can help to explain the fundamental mechanisms underlying complex, dynamical behavior with a high insight/complexity ratio. Importantly, this present analysis is limited to relatively fast, pulsatile and oscillatory flow of CSF over the surface of the brain and not the much slower, steady rates of production and absorption of CSF by the chorionic plexuses and arachnoid villi[18], conventionally seen as the mechanism of CSF flow.

The present oscillatory mechanism also helps to explain the existence, rationale, and survival value of the venous sinuses of the brain. These excessively large veins are covered by dura and surrounded by CSF, in a way that is not necessary for the return of venous blood to the heart. Their large cross sections and particular locations in the subarachnoid space may well have evolved to enhance their special volume compensation function.

The present simple and quantitative framework for describing basic time-varying relationships may allow greater understanding of the CSF flow as an intracranial “glymphatic” system[4,5]. Flow of CSF over the surfaces of the brain, especially during sleep, may be of profound importance in the movement and function of cell free fluid in the specialized lymphatic-like system for waste removal in the brain and spinal cord, which is structurally and functionally quite different from ordinary lymphatic drainage in extracranial tissues[10]. Dreaming may be a byproduct of brain activation necessary to drive autoregulatory changes in brain volume that, in turn, drive tidal movements of CSF. The necessary and refreshing nature of sleep has been attributed to the improved waste product removal[4,5].

Part of the pathophysiology of advanced Alzheimer’s disease and alcoholic encephalopathy may be related to slower tidal washing. As brain tissue volume shrinks from the original disease, the withs of the subarachnoid spaces increase[19]. In turn, the velocity of CSF movement over the cerebral convexities and the Virchow-Robbins spaces would diminish, leading to a slowing of removal of wastes such as Beta-amyloid [20], and even faster deterioration.

Another implication of the present hypothesis is that the mentally refreshing and mind clearing nature of aerobic exercise experienced by athletes may be due to increased amplitudes of both cardiac and respiratory components during strenuous exercise. Both pulse pressure and respiratory pressure swings in the chest can easily double in strenuous exercise[21]. Under these conditions CSF flow velocities over the cerebral cortex could approach those during sleep (Tables 3, 4, and 5) when the positive phases of unsynchronized cardiac and respiratory flows periodically add together. Perhaps the arcane mechanism described here helps to explain why strenuous exercise can be mentally restorative and improve cognitive function[22].

The present model in context

Heretofore, the challenge of understanding cyclic movement of cerebrospinal fluid has attracted a diverse community of investigators. Much attention has focused on pulsations at cardiac frequencies. Wagshul et al.[2] examined pulsatile flow of CSF associated with the systolic increase in blood pressure over the cardiac cycle in experimental and clinical studies. Rey and Sarntinoranont[9] characterized transfer functions between pulsations in arteries and pulsations in intracranial pressure. They found cardiogenic vessel pulses resulted in oscillatory CSF motion but no net flow over time. Thomas[10] used hydraulic network models to predict fluid motion produced by pulsation of perforating arteries and veins in the Virchow-Robbins spaces. Klarica and coworkers[23] described CSF movement correlated with the heartbeat "not as a circulation, but a rhythmic systolic-diastolic pulsation in all directions that promotes substance distribution inside the CSF system". However, pulsations over longer cycle times were not addressed. Recently, CSF pulsations at respiratory frequencies were studied by Vinje and coworkers[24], who found that in terms of volumetric flux (ml/sec), respiratory flows were equal to, or somewhat larger than, cardiogenic flows in amplitude, and appropriately slower in frequency (0.3 Hz).

High resolution computational fluid dynamics simulations of CSF motion have been described. Yiallourou et al.[25] studied and computationally modeled CSF motion in the cervical spine. Similarly Linge et al.[8] develop an idealized 3D computational model of the subarachnoid space of the posterior fossa and spinal canal (but not the cerebral convexities) and then used this model to predict CSF pressures and velocities. These models did not include CSF flow over the surfaces of the cerebral hemispheres and have numerous unknown parameters that need to be estimated.

Andreas Linninger and coworkers[7] described a comprehensive model of CSF flow throughout the cerebral ventricles and subarachnoid spaces surrounding the brain, not unlike the present model. In the Linninger model flow is induced by choroid plexus expansion rather than whole brain tissue expansion. That is, the authors "made the choroid plexus as the principal driver of CSF motion"[7]. Resulting transient increases in pressures of CSF in the cerebral ventricles lead to periodic compression of the brain parenchyma—the CSF volume expands and squeezes the brain. This dynamic is the reverse of that in the in the present model, where the brain volume expands and squeezes the CSF. Additionally, in the biophysics of Linninger et al. the ventricular wall is modeled as only thin layer of cells in the peri-ventricular area. This simplification allowed use of a thin elastic membrane model of tissue deformation. Importantly, the Linninger

model does not specify rigidity of skull. Volume compensation is provided by compression of an elastic brain such that in "each systole, the pulsations stretch the ventricles and SAS and, thus, elastic energy is stored. In effect, high systolic pressure loads the 'springs' of the elastic parenchyma …. this type of flow pattern can only occur in systems with distensible boundaries"[7].

The present model takes a different approach to organizing the cause-and-effect relationships among the principal players. The prime mover is pulsation of the brain blood volume caused by either cardiac action, breathing, or autoregulation. The brain expansion acts as a current source rather than a pressure source. Expansion is possible within the rigid box of the skull because it is drained via venous sinuses directly into the jugular veins and chest cavity at close to the lowest pressures in the cardiovascular system. The venous sinuses collapse as the total brain tissue within the skull expands and vis versa. Taken together, these mechanisms appear to capture the essence of complex CSF dynamics at three different time scales, both qualitatively and quantitatively.

Author contributions

Dr. Babbs is the sole author and is responsible for all aspects of the manuscript.

Conflict of interest statement

The author declares that there are no conflicts of interest.

Funding

This work was supported by Purdue University internal funds.

Acknowledgements

Inspiring informal conversations with colleagues at Purdue's Weldon School of Biomedical Engineering and their encouragement are gratefully acknowledged.

Data Sharing

The author is pleased to share all data and Excel spreadsheets with scientific colleagues upon request by E-mail.

References

1. Matsumae M, Kuroda K, Yatsushiro S, Hirayama A, Hayashi N, et al. (2019) Changing the Currently Held Concept of Cerebrospinal Fluid Dynamics Based on Shared Findings of Cerebrospinal Fluid Motion in the Cranial Cavity Using Various Types of Magnetic Resonance Imaging Techniques. Neurol Med Chir (Tokyo) 59: 133-146.
2. Wagshul ME, Eide PK, Madsen JR (2011) The pulsating brain: A review of experimental and clinical studies of intracranial pulsatility. Fluids Barriers CNS 8: 5.
3. Yang HS, Inglis B, Talavage TM, Nair VV, Yao JF, et al. (2022) Coupling between cerebrovascular oscillations and CSF flow fluctuations during wakefulness: An fMRI study. J Cereb Blood Flow Metab 42: 1091-1103.
4. Jessen NA, Munk AS, Lundgaard I, Nedergaard M (2015) The Glymphatic System: A Beginner's Guide. Neurochem Res 40: 2583-2599.
5. Benveniste H, Liu X, Koundal S, Sanggaard S, Lee H, et al. (2019) The Glymphatic System and Waste Clearance with Brain Aging: A Review. Gerontology 65: 106-119.
6. Mokri B (2001) The Monro-Kellie hypothesis: applications in CSF volume depletion. Neurology 56: 1746-1748.
7. Linninger AA, Tsakiris C, Zhu DC, Xenos M, Roycewicz P, et al. (2005) Pulsatile cerebrospinal fluid dynamics in the human brain. IEEE Trans Biomed Eng 52: 557-565.
8. Linge SO, Haughton V, Lovgren AE, Mardal KA, Langtangen HP (2010) CSF flow dynamics at the craniovertebral junction studied with an idealized model of the subarachnoid space and computational flow analysis. AJNR Am J Neuroradiol 31: 185-192.
9. Rey J, Sarntinoranont M (2018) Pulsatile flow drivers in brain parenchyma and perivascular spaces: a resistance network model study. Fluids Barriers CNS 15: 20.
10. Thomas JH (2019) Fluid dynamics of cerebrospinal fluid flow in perivascular spaces. J R Soc Interface 16: 20190572.
11. Damkier HH, Brown PD, Praetorius J (2013) Cerebrospinal fluid secretion by the choroid plexus. Physiol Rev 93: 1847-1892.
12. Boron WF, Boulpaep EL (2005) Medical Physiology. Philadelphia: Elsevier. 1319 p.
13. Fultz NE, Bonmassar G, Setsompop K, Stickgold RA, Rosen BR, et al. (2019) Coupled electrophysiological, hemodynamic, and cerebrospinal fluid oscillations in human sleep. Science 366: 628-631.
14. Zaharchuk G, Mandeville JB, Bogdanov AA, Jr., Weissleder R, Rosen BR, et al. (1999) Cerebrovascular dynamics of autoregulation and hypoperfusion. An MRI study of CBF and changes in total and microvascular cerebral blood volume during hemorrhagic hypotension. Stroke 30: 2197-2204; discussion 2204-2195.
15. Gauthier I, Hayward WG, Tarr MJ, Anderson AW, Skudlarski P, et al. (2002) BOLD activity during mental rotation and viewpoint-dependent object recognition. Neuron 34: 161-171.
16. Liang P, Shi L, Chen N, Luo Y, Wang X, et al. (2015) Construction of brain atlases based on a multi-center MRI dataset of 2020 Chinese adults. Sci Rep 5: 18216.
17. Bradley WG, Jr. (2015) CSF Flow in the Brain in the Context of Normal Pressure Hydrocephalus. AJNR Am J Neuroradiol 36: 831-838.

18. Khasawneh AH, Garling RJ, Harris CA (2018) Cerebrospinal fluid circulation: What do we know and how do we know it? Brain Circ 4: 14-18.
19. Double KL, Halliday GM, Kril JJ, Harasty JA, Cullen K, et al. (1996) Topography of brain atrophy during normal aging and Alzheimer's disease. Neurobiol Aging 17: 513-521.
20. Govindpani K, McNamara LG, Smith NR, Vinnakota C, Waldvogel HJ, et al. (2019) Vascular Dysfunction in Alzheimer's Disease: A Prelude to the Pathological Process or a Consequence of It? J Clin Med 8.
21. Ogoh S, Fadel PJ, Zhang R, Selmer C, Jans O, et al. (2005) Middle cerebral artery flow velocity and pulse pressure during dynamic exercise in humans. Am J Physiol Heart Circ Physiol 288: H1526-1531.
22. Tomporowski P, Ellis N (1986) Effects of exercise on cognitive processes: a review. Psychological Bulletin 99: 338-346.
23. Klarica M, Rados M, Oreskovic D (2019) The Movement of Cerebrospinal Fluid and Its Relationship with Substances Behavior in Cerebrospinal and Interstitial Fluid. Neuroscience 414: 28-48.
24. Vinje V, Ringstad G, Lindstrom EK, Valnes LM, Rognes ME, et al. (2019) Respiratory influence on cerebrospinal fluid flow - a computational study based on long-term intracranial pressure measurements. Sci Rep 9: 9732.
25. Yiallourou TI, Kroger JR, Stergiopulos N, Maintz D, Martin BA, et al. (2012) Comparison of 4D phase-contrast MRI flow measurements to computational fluid dynamics simulations of cerebrospinal fluid motion in the cervical spine. PLoS One 7: e52284.